Investigation of fragment reconstruction accuracy with *in situ* few-view flash x-ray high-speed computed tomography (HSCT)

OPEN ACCESS
IOP Publishing

Made open access 3 April 2020
Measurement Science and Technology

Meas. Sci. Technol. **30** (2019) 065401 (8pp)

https://doi.org/10.1088/1361-6501/ab11bb

Investigation of fragment reconstruction accuracy with *in situ* few-view flash x-ray high-speed computed tomography (HSCT)

Stefan Moser[1], Siegfried Nau[1], Victoria Heusinger[1] and Michael Fiederle[2]

[1] Fraunhofer Institute for High-Speed Dynamics, Ernst-Mach-Institut, EMI, Am Klingelberg 1, 79588 Efringen-Kirchen, Germany
[2] Albert-Ludwigs-Universität Freiburg, FMF, Freiburger Materialforschungszentrum, Stefan-Meier-Strasse 21, D-79104 Freiburg, Germany

E-mail: stefan.moser@emi.fraunhofer.de

Received 31 August 2018, revised 4 March 2019
Accepted for publication 20 March 2019
Published 16 April 2019

Abstract

Few-view *in situ* flash x-ray high-speed computed tomography (HSCT) is a computed tomography (CT) technique used to investigate high-speed phenomena on the timescale of microseconds. The successful application to quantitatively analyze and characterize fragments formed during a 1000 m s^{-1} impact process onto a ceramic plate with a CT reconstruction from only six x-ray projections has been shown. The method delivers spatially resolved 3D information about the fragments at one point in time. This information is not (or only partially) accessible by alternative experimental methods. Therefore, quantifying the accuracy of the measured data is not directly possible. In order to estimate the precision of the method and the influence of different sources limiting accuracy, a simulation study consisting of 250 virtual experiments was carried out. The border conditions of the study are based on the actual experimental data from the six-view experiment. The results show that steel fragments with a diameter of about 8 mm (volume ~ 300 mm^3, weight ~ 2.5 g) can be reconstructed with an averaged relative volume deviation of about 30%. For larger frements, the error reduces down to 10% relative average deviation. The spatial position of the center of mass can be determined with an averaged uncertainty of about 0.8 to 1.2 mm for most fragment sizes.

Keywords: HSCT, algebraic reconstruction, flash x-ray, computed tomography, *in situ* imaging, impact processes, sparse datasets

(Some figures may appear in colour only in the online journal)

1. Introduction and motivation

Computed tomography (CT) has long left behind its roots in medical applications [1] and has become an important measurement method in science and technology. [2]. However, the application to dynamic processes is still a challenge for many applications [3, 4]. Conventional CT methods rely on the sequential acquisition of the images of one dataset for reconstruction (usually several hundred projections) during a timeframe in which the investigated object is in a quasi-static state [5, 6]. This is necessary to give a spatially and temporally consistent dataset for reconstruction. The current state of the art for the time limit using high-flux x-ray sources like synchrotrons is on the order of one second [7] to acquire a full dataset.

For faster processes on the scale of microseconds, e.g. the investigation of impact processes, usually flash x-ray technology is employed [8, 9]. However, this classic radiography technique allows a 2D analysis only. From other application areas, e.g. optical flow tomography, the application of ART-type algorithems for tomographic reconstruction based on few projections also is an established method [10, 11]. For small-scale problems, electron-beam scanning devices have been developed [12]. To overcome this limitation and acquire tomographic 3D

information for high-speed phenomena in ballistics, few-view high-speed computed tomography (HSCT) has been developed over the last years [13–15]. The core aspect of this technique is to acquire all images parallel at one point in time. To realize this, multiple synchronized flash x-ray tubes (allowing illumination times as short as 20 ns) and the same number of detectors are employed. However, this approach comes with restrictive experimental boundary conditions, the most obvious one being the severe limitation in the number of projections. While conventional NDT CT methods usually acquire between 400 and 1600 projections, HSCT usually is realized with 3–10 projections. Newer setups consist of up to 15 source-detector pairs [16]. Nevertheless, these extremely low projection numbers lead to very strongly under-sampled datasets. Usually, artefacts are present in the reconstruction results, which restricts the method to high-contrast problems. To mitigate this, algebraic reconstruction algorithems [17, 18] are employed for reconstruction. The reason is, that these are much more robust towards missing information and mediocre image quality than the classical Feldkamp type algorithms [19, 20].

In [21] the successful application of the HSCT technique with six projections was demonstrated. The problem investigated was the quantitative analysis of a high-speed (1000 m s^{-1}) impact process of a steel cylinder on a ceramic plate. The scope of the investigation was to reconstruct the fragment cloud after the impact at one point in time. The means was to characterize the size (volume) and spatial position of the individual fragments from a 3D reconstruction. From this data, information like mass, velocity vector, impulse and kinetic energy of each individual fragment can be derived.

A quantitative analysis of the accuracy of this information could not be carried out with the data available. Therefore, this question remained open and was therefore also was the focus of the paper reviews.

The scope of this paper is to analyse the accuracy that can be achieved with this particular experimental setup by desiging and carrying out a simulation study. The goal is to give an estimate of the plausibility of the 3D reconstruction of a dynamic event from few flash x-ray projections.

1.1. Experimental image acquisition and tomographic reconstruction

The experimental setup used for image acquisiton consists of six flash x-ray tubes operating at 450 kV with a lead collimator of 20 mm thickness to reduce cross-illumination. The detectors were realized by commercialy available 1050 × 350 mm and 900 × 300 mm storage detector screens, resulting in cone beam projection images. One channel was composed of two detector sheets, resulting in five 1050 × 700 mm and one 900 × 600 mm active detector areas. The detectors were sandwiched between wooden plates of 12 mm thickness for a compromise between physical protection and imaging quality. For further protection of the setup, the impact area was encased inside a 200 mm diameter plastic tube. Source-screen distances were between 1770 and 2260 mm. The overall setup was constructed as a circular arrangement perpendicular to the movement axis of the steel cylinder. One additional channel was added oriented as close as possible to the shooting axis. See figure 1 for details.

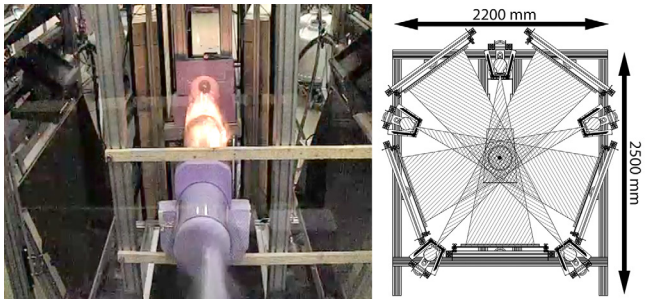

Figure 1. Left: optical image of the experiment taken during impact (frame extracted from video). Here, a transparent plastic protection tube was used to allow optical investigation. Right: technical drawing of the experimental setup for the five channels perpendicular to the shooting direction. Reproduced from [21]. © IOP Publishing Ltd. All rights reserved.

For reconstruction, an AVMART-type algebraic tomography reconstruction algorithm was used, since multiplicative algorithms show robustness and performance for undersampled datasets [22]. Due to the large source-detector distances and the specifications of the flash x-ray tubes, high levels of noise and blurring in the images was observed. Since the low number of projections does not lead to an averaging out of these influences, a regularization mechanism is usually employed for this class of inverse problems [23]. Therefore, the AVMART algorithm was extended by a splatting [24] type regularization mechanism described in [21] to increase stability of the results and reduce artifacts.

The images were acquired from the hardware by digitizating the storage screens with a resolution of 3.1 pixels mm^{-1} with a commercially available medical digital radiography scanner. In an additional step, the images were corrected for geometrical distortions during the digitization process (on the scale of 5 mm in scanning direction and −2 mm perpendiculat for the 1050 × 350 mm detectors). Then a logarithamization the grey values was carried out to prepare the images for the processing by the reconstruction code.

1.2. Methodical approach: simulation study

Since a direct experimental comparison of the results to reference data is not possible for the reasons discussed in 1.1, a simulation study approach was chosen. This also allows to investigate several experimental aspects separately.

On of them is the correlation between the (random) orientation of the fragments and the (fixed) orientation of the experimental setup, which plays a significant role [25].

One of the benefits of a simulation study therefore is the ability to identify the most promising approaches to advance the HSCT technique by identifying the most prominent degrading influences. Therefore, the extended scope of this paper is to assert the individual and combined impact of quality-limiting effects of HSCT and to derive and assess promising approaches to improve the method.

Figure 2. Exemplary image of the steel cylinder before impact (leftmost item) and the three largest fragments formed during an impact process (to the right). Reproduced with permission from [26].

1.3. Reference data for the evaluation

The number of x-ray projections, the acquisition geometry and the shapes and materials of the object (in this case, the fragments and remnants of the ceramics plate) are one of the biggest influences on the reconstruction quality. For the given experiment, these are fixed border conditions and not subject of the scope of this paper. However, these aspects will be discussed in the conclusion and outlook.

To estimate the influence of the other error sources as realistically as possible for the given experiment, seven real fragments of different sizes and shapes formed during an actual experiment were chosen as reference objects (see figure 2) in favour of a generic reference object.

2. Border conditions and investigated parameters for the simulation study

Presumably four main influences to achivable reconstruction quality can be derived:

- Few projections: Probably one of the most important aspect of few-view HSCT is the fact that the reconstruction has be carried based on a strongly undersampled dataset, in this case six projections. This corresponds to the 'basic' error of the investigated experiment that cannot be reduced further for this experimental setup. Therefore, this influence is treated as an existing border condition that is not investigated further.
- Flash x-ray tube spot size: the spot size of flash x-ray tubes used for the experiment (energies at 450 kV) are usually approximately one millimeter in diameter [27]. This leads to a blurring of the images.
- Geometric errors: one of the practical problems of HSCT is—severity depending on the application—the necessary relative and absolute geometric calibration of the position of the sources and detectors. To address this issue, a photogrammetry-based method was used in [21] to calculate the exact geometry setup directly from the images. However, the precision of this method has empirically turned out to have a residual uncertainty of about one millimetre for the source and screen positions.
- Image noise: due to the source-screen distance of about two meters and the serious issue of scatter and cross-scatter, the quality of the x-ray images is only moderate. Despite image post-processing (adapted flat-field image correction), the signal-to-noise ratio (SNR) of the images can be as low as about 30. This leads to additional errors in the reconstruction, that can only be reduced to some degree by regularization methods in the 3D reconstruction step.

The experimental realization of course is influenced by more than these four aspects. Among them are e.g. errors and image artefacts that can be caused by the digitization of the storage screens, influences on local contrast and structures due to scatter, shielding, or physical protection measures. The aspects of spatially dependent contrast degradation are intrinsically included in the simulation by setting the optical input densities based on the actual reconstruction results (this is discussed in the 'methods' section). The other experimental influences are, compared to the four aspects discussed in the list above, estimated to be less severe than the four main influences. Therefore they are left out of the picture for the following analysis.While the basic approach and preliminary results are discussed in [26], an in-depth analysis with larger datasets and the additional inclusion of noise as an error source has been carried out for this paper and will be discussed in the following chapters.

3. Methods

The simulation study was carried out in three steps: semi-random generation of a synthetical input volume and generation of images; introduction of error contributions, and evaluation.

3.1. Input volume and image generation

The creation of the synthetic representative volumes is divided in two steps. First, a digital, simplified static representation of the objects in the reconstruction volume that are not relevant for the evaluation (everything but the fragments) was created based on the reconstructed densities drawn from the actual reconstruction results. In the second step, seven fragment subvolumes were placed at random positions and orientations in the volume.

This step was realized by an automated script that uses a random number generator to create arbitrarily distributed fragment positions and orientations. This placement process was limited to the spatial volume, where the fragment cloud is expected based on the actual experimental data. Since the exact fragment placement and orientation is a statistically random process, 50 randomly calculated volumes that differ regarding the exact position and angular orientation of the fragments were created. The reference fragment subvolumes are the results of conventional high-resolution NDT 3D-CT scans with a conventional CT device of the recovered steel fragments from an actual experiment shown in figure 2. For an example of the CT reconstruction, see figure 3.

All results presented in this paper are based on the automated, statistical evaluation of these 50 created volumes. Slice images with comparable segmentation of an actual

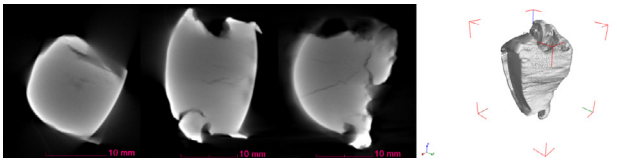

Figure 3. Conventional high resolution (40 μm voxel size) NDT Computed Tomography reconstruction of the largest fragment from figure 2. Left: slice images, right: 3D render image.

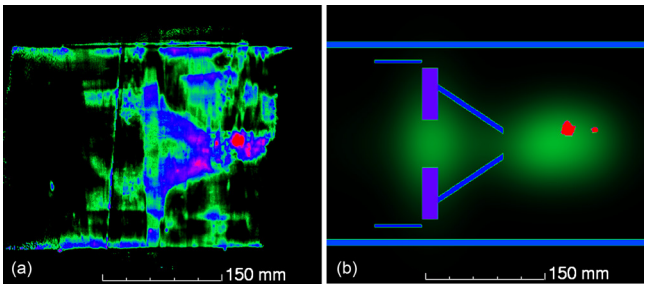

Figure 4. (a) *XY* Slice image from actual reconstructed volume. Reproduced from [21]. © IOP Publishing Ltd. All rights reserved. (b) Slice image from a synthetically generated volume. From the seven fragments, only two are visible in this slice. While (a) is an actual reconstruction containing numerous artefacts, (b) is generated artefact-free for the projection generation (reproduced with permission from [26]).

experimental result and a synthetically created volume are shown in figure 4.

These 50 different input volumes were used in the following step as a basis to create simplified x-ray projections by using the forward projection kernel of the reconstruction algorithm, see figure 5.

While the synthetically created volume files have a resolution of 2.49 voxels per mm, the reconstruction is carried out with a lower resolution of 1.0 voxels per mm (identical to the reconstructions from actual experimental data evaluated in [21]). The reason for the higher volume resolution for image generation than in reconstruction is to avoid the 'inverse crime'. This is known to lead to unrealistically good results in simulation studies when using identical resolutions both for image generation as well as reference for evaluation [28].

3.2. Introduction of experimental error sources

The synthetically generated reference volumes are the basis for the creation of synthetical x-ray image datasets. Each dataset consists of six forward projections according to the geometric arrangement used in the actual experiment. To investigate the influence of different image quality degrading influences, following imaging datasets were generated for each individual reference volume:

- 'regular': quasi-ideal forward projection images without error influences
- 'blurred': projection images including the one millimetre diameter spot-size (modelled as a Gaussian profile)
- 'noise': projection images with added Gaussian white noise with an effective SNR of 30
- 'combined': projection images with these two effects combined.

The CT reconstruction was carried out with parameters corresponding to the evaluation in [21]. These are regularization parameter $s = 0.8$, relaxation parameter $\mu = 0.1$, 50 iterations and voxel size 1 mm.

In order to investigate the effect of geometrical errors on the reconstruction precision, two additional studies of the same 50 volumes have been carried out using the image data from the 'regular' and the 'combined' datasets. In these reconstructions, additional geometric errors were introduced by randomly varying all source and detector coordinates independently in the range of $\pm$ (0, …, 1) mm in X, Y and Z direction (the coordinates-modified datasets are abbreviated 'cmod' in the following).

This approach lead to 5 sets of 50 reconstructions each:

- 50 'regular' reconstruction based on quasi-ideal forward projections without error influences
- 50 'blurred' reconstruction based on projections including the blurring due to the x-ray source spot-size
- 50 'noise' reconstruction based on projections with added Gaussian white noise with an effective SNR of 30
- 50 'regular-cmod' reconstruction based on quasi-ideal forward projections, but with a $\pm$ (0, …, 1) mm random offset in source-detector-positions between acquisition and reconstruction geometry
- 50 'combined' reconstructions based on projection datasets with the two image quality reducing effects (blurring and noise) as well as the $\pm$1 mm random position modification.

Every reconstruction (1, …, 50) of a set is directly comparable to the reconstruction with the same number from another set, because it is based on the same input volume.

To analyze the deviations, the 250 reconstructions were analyzed regarding volume and center-of-mass position of the fragments. These values then were compared to the known reference values (given by the input volume). This comparison allows the differentiation between the individual and the combined (total) error contributions of the respective influences.

3.3. Evaluation

The reconstruction was carried out with the AVMART reconstruction algorithm for all 250 datasets with identical parameters. The evaluation was also carried out with an automatic method identical for all volumes.

In the first step, for each reconstruction result, the volume-specific voxel-density threshold value to identify fragments in the respective volume was determined automatically. This value is defined as the voxel density value for which the number of voxels above the threshold in the central area of the reconstruction volume, multiplied with the volume associated with one voxel, is equal to the known volume of the fragment before impact. This approach can be viewed as using *a priori* information about the known volume of high-contrast material in the system as a border condition for threshold calculation. This *a priori* information is available in the actual experiment as well as in thie simulation study.

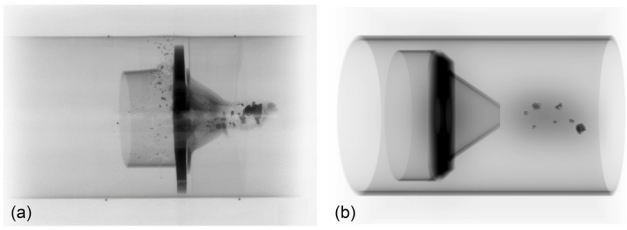

Figure 5. (a) Actual x-ray projection from the experiment. (b) One of the 'regular' projection images generated from a synthetically created volume ((a) reproduced from [21]. © IOP Publishing Ltd. All rights reserved. (b) Reproduced with permission from [26]).

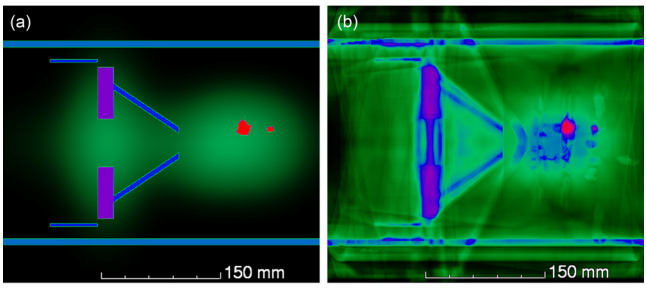

Figure 6. (a) *XY* slice through the input volume. (b) *XY* slice at the same location through the reconstruction result from six projections in the regular case (reproduced with permission from [26]). Artefact structures correspond to the actual experiment (figure 4(a)).

In the ideal case (e.g. hundreds of projections and not an undersampled dataset), this threshold value should be identical for all volumes. However, due to the semi-random placement of the fragments, this threshold value varies depending on the individual artifact structure and the smearing out of the density over the volume. Therefore, the threshold was calculated for each volume individually.

This makes sure that only the voxels with the highest density are available for evaluation and at the same time acts as an efficient supressing method for artefacts. The reason for this is that—independent from the individual shape—the reconstruction artifacts usually have a significantly lower density as the voxels containing the fragments, due to the high physical density and absorption of the steel, resulting in a high contrast. (see figures 4 and 6).

The actual evaluation for each fragment also was carried out individually to allow an individual analysis of the results:

For each fragment, a sub-volume centered on the known location of the respective fragment was extracted from the original (input) volume (scaled down to the lower voxel resolution of the reconstructed volume) as well as from the reconstructed volume (the reconstruction result).

These two subvolumes containing the individual fragments were compared to each other regarding the number of voxels above the specific density threshold for the volume (yielding the actual mass of the fragment and the deviation from the reference mass) as well as the center of mass (giving the deviation of the location of the fragment from the reference).

The result of these comparisons was evaluated for each individual fragment regarding the absolute error in volume and spatial position (allowing to estimate the absolute precision of the method) as well as the average size of the deviation.

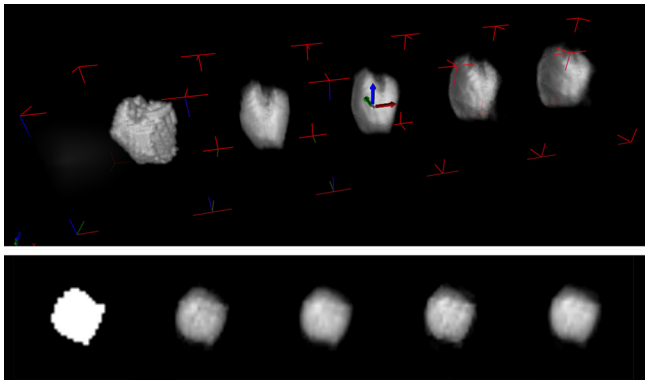

Figure 7. 3D-render images (top) and 2D slice images (bottom) for the largest fragment. From left to right: reference, regular reconstruction, blurred, cmod and combined. The segmentation and orientation is identical for all fragments. The reference slice image (bottom left) appears to be binary, because the fragment is of homogeneous density in the reference volume.

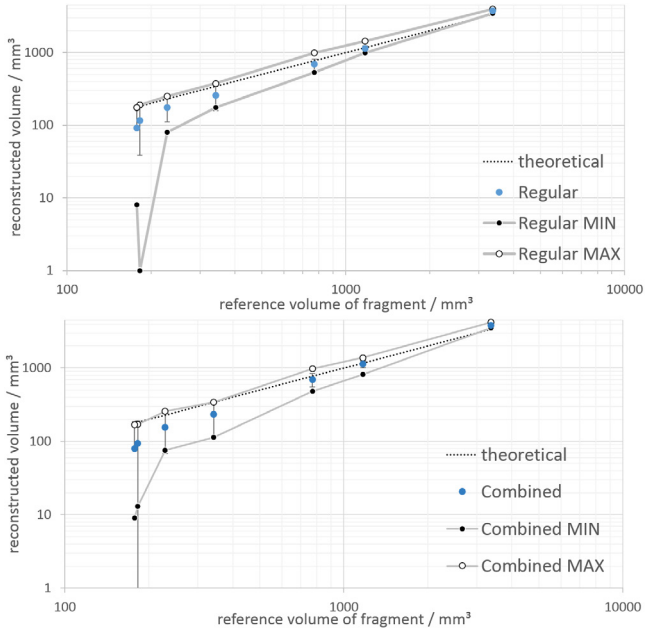

Figure 8. Plot of average fragment volumes for the regular case (top) and the combined case (bottom) as well as the respective min/max values for the 50 reconstructions carried out for each block.

Overall, 7 fragments × 50 volumes × 5 sets = 1750 fragments were analyzed with this method.

4. Results and discussion: volume and centre of mass location errors

4.1. Evaluation of reconstructed fragment volumes

An example for a reconstructed fragment is shown in figure 7, including the reference (leftmost item).

In figure 8, the averaged and min/max reconstructed fragment volumes for the regular case and the combined case (including all four discussed error sources) are shown. The first and most important observation is, that the absolute deviation of the results from the known reference is significant and

large, compared to the fragment sizes in the regular, as well as in the combined case. The average fragment volume error is less severe for the regular case. This confirms the expectation, that a reconstruction from only six projections results in significant artefacts and therefore the 'baseline error' discussed earlier is significant. This error is increased when additional error sources are included, which also meets expectations.

Also noteworthy is the fact that—in one of the 'regular' cases—one of the smaller fragments (below 200 mm^3) is reconstructed with a volume of only one voxel. This means it could be classified as an artefact and ignored in an evaluation of experimental data. These results show that is possible to dramatically underestimate (or not detect at all) small fragments. This lower bound volume corresponds to a diameter of about 7 mm for a sphere, but usually fragments of this size are elongated shards that are not spherical (as the exemplary fragment used in this study) and therefore—depending on their orientation in space—significantly harder to reconstruct consistently.

The study also shows that the reconstruction of smaller fragments is consistently for all cases too small. On average, they are reconstructed with only 50% of their volume as compared to fragments with a volume of about 200 mm^3. This behavior can be easily explained. Since one of the main artefacts types due to the undersampling is a blurring of the reconstructed fragments edges, this results in a 'smearing out' of the density to adjacent voxels (compare figure 6). The smaller the fragment size is, the more severe the effect is relative to fragment size. The size of larger fragments, on the other hand, is overestimated. This behavior is also expected, since the overall fragment volume is known and set as a boundary condition by the user for the evaluation via the threshold. If the small fragments are underestimated, the larger fragments have to be overestimated.

In figure 9, the averaged errors for the different fragments and reconstruction modes are shown. The relative error of the reconstructed volume sizes (part (a)) confirms the fact, that the average relative volume error is especially large for small fragments and smaller for larger fragments. This is expected, since larger, more prominent structures can be reconstructed even with limited data, while fragments of a very small size get obscured and hidden by other structures much more easily.

The direct comparison of the influence of the different error sources confirms the fact, that the main influence on the error comes from the undersampling due to few projections. Even in the ideal case, the smallest fragments have an average error of 50% volume-wise, dropping to below 30% for fragments above the order of magnitude of 200 to 300 mm^3.

Of the individual error sources it comes as a surprise, that noise seems to have the least effect on the volume size of the three different influences. The regularization employed in the reconstruction algorithm seems to handle that influence rather efficiently. As expected, the blurring due to the x-ray flash tube spot size and the geometric uncertainty has a significant impact on volume reconstruction precision. All error sources combined yield the largest error, as is expected, increasing the average volume deviation by up to an additional 10% for the smaller fragments.

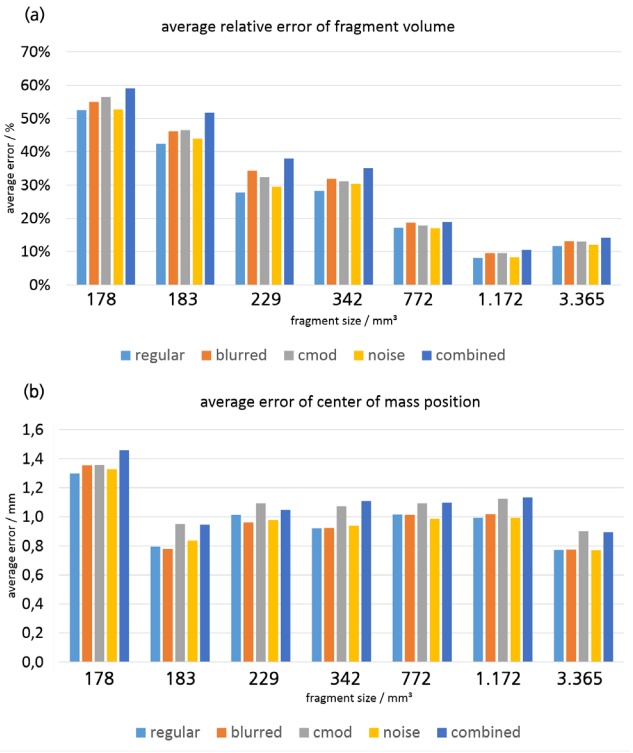

Figure 9. Errors averaged over 50 individual reconstructions of ((a), top) the fragment volume and ((b), bottom) the center of mass position; shown for the five different reconstruction modes (regular, blurred, cmod, noise and all error sources combined).

4.2. Evaluation of centre of mass positions

In part (b) of figure 9, the averaged deviations for the center of mass position is shown. The average deviation is on the order of magnitude of 1 mm for all fragment sizes.

Noise and blurring do not seem to have a measurable impact on the localization of the fragments. The influence of the geometric uncertainty however is clearly visible and increases the average absolute error of the center of mass position by about 0.1 to 0.2 mm for all fragment sizes. This can be explained by the fact, that blurring and noise are spatially isotropic and therefore primarily affect the sharpness of the fragment boundary (reducing volume precision). This does not have a large influence on the actual position of the center of mass, which is determined by calculating the arithmetic average of the coordinates of all voxels associated with the fragment. For most fragments though, the averaged error when considering all error sources is larger than the influence of the geometric uncertainty alone.

5. Conclusion and outlook

5.1. Summary and conclusion

In this paper, it was attempted to give an estimate of the accuracy (mean deviation from the true values) of the results calculated from a tomographic reconstruction of a high-speed CT dynamic impact event. The values investigated were the mass and position of the fragments. The investigation was carried

out for one particular implementation of a given experimental HSCT setup with six projection channels.

For this study, ideal projection images, images with added white noise equivalent to experimental data (SNR 30), blurred images due to the imaging system properties (spot size diameter of the x-ray flash tubes used in the experiments approx. 1 mm) were generated. Tomographic reconstructions considering geometric uncertainty of the input data as expected in the actual experiment ± 1 mm, as well as all of these effects combined, were carried out with these images.

The investigations suggest that using six projections, fragments with a volume larger than about 300 mm^3 can be reconstructed with an average relative volume deviation of about 30% to 40% to the true value (decreasing with increasing fragment size down to about 10% for fragments with a volume $> 3000\,mm^3$). The position of the fragments (center of mass) at the time of image acquisition can be determined with average deviations of 0.8 to 1.2 mm from the true value for all fragment sizes, with a tendency of smaller deviations for larger fragments.

The results show that the main error in volume determination comes from the undersampled nature of the dataset consisting of only six projections. The influence of the other experimental error sources is small in comparison to this 'baseline error' due to the given properties (fixed geometry and fixed number of projection channels) of the setup.

The analysis leads to the conclusion, that optimizing the acquisition geometry is a central aspect when designing a HSCT setup for the investigation of high-speed events.

5.2. Outlook

The simulation study method presented in this work has been shown to be a suitable method to quantify the perfocmance of a given acquisition geometry for a given experiment. This means, that the method could be used to calculate a calibration for given experimental setups. An example for the experiment discussed in this publication would be to calculate a volume-dependent correction factor to compensate the consistent under-estimation of small and the over-estimation of large fragment volumes.

The method also could be used to optimize the acquisition geometry of newly constructed experimental HSCT setups in advance, if preliminary imaging data (e.g. from a single-channel setup) and post-mortem information is available.

One of the key aspects in optimizing HSCT setups is adding more projection channels, as has been realized by Zellner *et al* [16]. This approach allows another approach: accepting reduced reconstruction accuracy for dynamic information. This is realized by acquiring multiple imaging datasets from one experiment by triggering only a subset of source-screen pairs at a given time. The simulation framework presented in this publication could be applied to the existing setup, allowing to predict the optimal tradeoff for projection numbers per sub-dataset versus volume precision for different applications with varying complexity.

Acknowledgments

The authors wish to thank the staff of the EMI experimental facilities Kandern, foremost Dr Christoph Glößner, Dipl. Ing. FH Klaus Sütterlin, Dipl. Ing. FH Gregor Popko and MSc Ralph Langkemper for their work and support involved in preparation and carrying out the experiment. Further, the authors thank the anonymous referees for their valuable input.

ORCID iDs

Stefan Moser https://orcid.org/0000-0002-0668-7435

References

[1] Pan X, Siewerdsen J, La Riviere P J and Kalender W A 2008 Anniversary paper: development of x-ray computed tomography: the role of medical physics and AAPM from the 1970s to present *Med. Phys.* **35** 3728–39
[2] Zabler S, Fella C, Dietrich A, Nachtrab F, Salamon M, Voland V, Ebensperger T, Oeckl S, Hanke R and Uhlmann N 2012 High-resolution and high-speed CT in industry and research *Proc. SPIE* **8506** 850617
[3] Buffiere J Y, Maire E, Adrien J, Masse J P and Boller E 2010 *In situ* experiments with x-ray tomography: an attractive tool for experimental mechanics *Exp. Mech.* **50** 289–305
[4] Stürzel T, Bieberle M and Hampel U 2011 A device for ultrafast three-dimensional x-ray computed tomography with a scanned electron beam *IEEE Nuclear Science Symp.* pp 25–9
[5] Berg S *et al* 2013 Real-time 3D imaging of Haines jumps in porous media flow *Proc. Natl Acad. Sci. USA* **110** 3755–9
[6] Rack A, Garcia-Moreno F, Baumbach T and Banhart J 2009 Synchrotron-based radioscopy employing spatio-temporal micro-resolution for studying fast phenomena in liquid metal foams *J. Synchrotron Radiat.* **16** 432–4
[7] Mokso R, Marone F, Haberthur D, Schittny J C, Mikuljan G, Isenegger A and Stampanoni M 2011 Following dynamic processes by x-ray tomographic microscopy with sub-second temporal resolution *10th Int. Conf. on X-Ray Microscopy* vol 1365 pp 38–41
[8] Schuster B E, Aydelotte B B, Leavy R B, Satapathy S and Zellner M B 2015 Concurrent velocimetry and flash x-ray characterization of impact and penetration in an armor ceramic *Proc. of the 2015 Hypervelocity Impact Symp.* ed W P Schonberg (Amsterdam: Elsevier) pp 553–60
[9] Strassburger E, Hunzinger M, Patel P and McCauley J W 2013 Analysis of the fragmentation of AlON and spinel under ballistic impact *J. Appl. Mech.-Trans. ASME* **80** 11
[10] Medhi B, Hegde G M, Reddy K P J, Roy D and Vasu R M 2015 *Orthogonal Projection Based Computationally Efficient Algorithm for Deflection Tomography in High Speed Flow Studies 29th Int. Symp. on Shock Waves (ISSW 2013)* pp 459–64
[11] Zhang B, He Y, Song Y and He A 2009 Deflection tomographic reconstruction of a complex flow field from incomplete projection data *Opt. Lasers Eng.* **47** 1183–8
[12] Bieberle M, Barthel F, Menz H-J R, Mayer H-G and Hampel U 2011 Ultrafast three-dimensional x-ray computed tomography *Appl. Phys. Lett.* **98** 3
[13] Zoltani C K, White K J and Di Bianca F A 1986 Flash x-ray computed tomography facility for microsecond events *Rev. Sci. Instrum.* **57** 602–11

[14] Thoma K, Helberg P and Strassburger E 2007 Real-time resolved flash x-ray cinematographic investigation of interface defeat and numerical simulation validation *23rd Int. Symp. on Ballistics (Taragona, Spain)* pp 1065–72
[15] Mentzer M A and Gurganus J C 2012 Design and analysis of a cineradiographic x-ray imaging system for capturing dynamic deformation of materials *Opt. Eng.* **51** 11
[16] Zellner M B *et al* 2017 Development of a multi-energy flash computed tomography diagnostic for three dimensional imaging of ballistic experiments *Proc. of the Shock Compression of Condensed Matter Topical Group Meeting of the American Physical Society* (St. Louis, Mo: AIP Conference Proceedings) p 10
[17] Gordon R, Bender R and Herman G T 1970 Algebraic reconstruction techniques (ART) for three-dimensional microscopy and x-ray photography *J. Theor. Biol.* **29** 471–81
[18] Gilbert P 1972 Iterative methods for the three-dimensional reconstruction of an object from projections *J. Theor. Biol.* **36** 105–17
[19] Pan X, Sidky E Y and Vannier M W 2009 Why do commercial CT scanners still employ traditional, filtered back-projection for image reconstruction? *Inverse Problems* **25** 123009–45
[20] Feldkamp L A, Davis L C and Kress J W 1984 Practical cone-beam algorithm *J. Opt. Soc. Am.* **1** 612–9
[21] Moser S, Nau S, Salk M and Thoma K 2014 *In situ* flash x-ray high-speed computed tomography for the quantitative analysis of highly dynamic processes *Meas. Sci. Technol.* **25** 11
[22] Mishra D, Longtin J P, Singh R P and Prasad V 2004 Performance evaluation of iterative tomography algorithms for incomplete projection data *Appl. Opt.* **43** 1522–32
[23] Gross D, Heil U, Schulze R, Schoemer E and Schwanecke U 2010 GPU-based volume reconstruction from very few arbitrarily aligned x-ray images *SIAM J. Sci. Comput.* **31** 4204–21
[24] Zwicker M, Pfister H, van Baar J and Gross M 2001 EWA volume splatting *IEEE Visualization (San Diego)* pp 29–36
[25] Zheng Z and Mueller K 2011 Identifying sets of favorable projections for few-view low-dose cone-beam CT scanning *Fully 3D Image Reconstruction in Radiology and Nuclear Medicine* (Potsdam, Germany) p 4
[26] Moser S 2017 Computertomographie mit stark unterbestimmten Datenstätzen für komplexe Anwendungen, Albert-Ludwigs Universität Freiburg, Fakultät für Umwelt und natürliche Ressourcen *PhD Thesis* Fraunhofer Verlag p 240
[27] Scandiflash AB 1993 *Instruction Manual Scandiflash Model 450* p 65
[28] Kaipio J and Somersalo E 2007 Statistical inverse problems: Discretization, model reduction and inverse crimes *J. Comput. Appl. Math.* **198** 493–504